Mechanical Systems and Signal Processing 208 (2024) 111012

Contents lists available at ScienceDirect

Mechanical Systems and Signal Processing

journal homepage: www.elsevier.com/locate/ymssp

Design, tuning and in-field validation of energy harvesters for railway bridges

J.C. Cámara-Molina [a,*], A. Romero [a], E. Moliner [b], D.P. Connolly [c], M.D. Martínez-Rodrigo [b], D. Yurchenko [d], P. Galvín [a,e]

[a] Escuela Técnica Superior de Ingeniería, Universidad de Sevilla, Camino de los Descubrimientos s/n, ES-41092, Sevilla, Spain
[b] Universitat Jaume I, Department of Mechanical Engineering and Construction, Avda. Sos Baynat s/n, ES-12071, Castellón, Spain
[c] School of Civil Engineering, University of Leeds, UK
[d] Institute of Sound and Vibration Research, University of Southampton, Southampton SO17 1BJ, UK
[e] ENGREEN, Laboratory of Engineering for Energy and Environmental Sustainability, Universidad de Sevilla, Camino de los Descubrimientos s/n, ES-41092, Sevilla, Spain

ARTICLE INFO

Communicated by J.E. Mottershead

Keywords:
Piezoelectric energy harvesting
Railway bridges
High-speed train
Tuning frequency

ABSTRACT

Energy harvesters are a promising technology for powering infrastructure condition monitoring systems without batteries. When deployed on railway bridges they are typically tuned to the bridge's natural frequency, however due to the dominance of train-induced forced vibration of the structure, this results in sub-optimal energy harvesting. As a solution, this paper presents a novel tuning strategy for energy harvesters on railway bridges. The strategy is based on a statistical analysis of the mechanical energy generated in the bridge during train passage and involves four steps: (*i*) measurement of bridge response due to train traffic, (*ii*) calculation of mechanical energy during train passage, (*iii*) statistical characterisation of the energy distribution, and finally, (*iv*) calculation of the tuning frequency. A case study is presented to compare the potential of the proposed strategy against tuning based upon the bridge natural frequency. First, an in-service railway bridge is monitored to determine its natural frequency and response to train traffic. Combining the field data with the proposed tuning strategy, the design of energy harvesters for the bridge is optimised. The design of harvesters tuned to natural frequencies is also studied. The underlying harvester type is a cantilever bimorph beam with a mass at the tip and load resistance. Additive manufacturing is used for the substructure, which is formed from PAHT-CF15 (High Temperature Polyamide carbon fibre reinforcement). The harvesters are manufactured and deployed on the bridge subject to live railway traffic. Field results show the devices designed using the new tuning strategy harvest up to 300% more energy. The energy harvested in a time window of three hours (18 train passages) is 7.65 mJ.

1. Introduction

The use of autonomous and real-time infrastructure condition monitoring systems for railways offers financial and safety-related benefits to operators. In recent decades, the development of the Internet of Things (IoT) has allowed new wireless communication protocols and gained the attention of the scientific community [1,2]. The application of IoT for real-time structural health monitoring (SHM) has been successfully implemented in buildings and civil engineering infrastructures, in historic buildings, bridges, civil

* Corresponding author.
E-mail address: jcamara@us.es (J.C. Cámara-Molina).

https://doi.org/10.1016/j.ymssp.2023.111012
Received 7 June 2023; Received in revised form 29 August 2023; Accepted 3 December 2023
Available online 8 December 2023

structures, and soils [3–5]. Recent advances in SHM deployments in rail systems have been revised by Barke and Chiu [6], Vagnoli et al. [7], and Jing et al. [8]. SHM systems allow new developments in predictive maintenance strategies to assess the serviceability condition of rail systems without traffic disruption and at reduced costs. However, one of the main challenges with monitoring systems is the need for a reliable power supply. Lack of access and maintenance operations in remote areas can limit their practical implementation [9].

Energy harvesting from ambient vibrations is an alternative to traditional battery power for the sensors and nodes in monitoring systems [9–11]. For instance, Rodriguez et al. [12] developed an IoT sensor powered by vibrations from industrial air compressors without the need for a battery. The energy harvester was tuned to the dominant frequency of the vibrations of the compressor by adjusting the geometrical design parameters. Then, the system was able to power a sensor with a duty cycle of 30 s. Although energy harvesting devices are a promising solution for powering autonomous monitoring systems from ambient vibration, a challenge in the design is the reduced operating range close to the resonant or tuning frequency [13]. Maximum performance is achieved for energy harvesters tuned to the excitation frequency, and slight deviations from the resonance condition cause a drastic reduction in the output power.

Solutions for efficiency reduction due to frequency detuning are based on increasing the operating frequency bandwidth and tuning the resonant frequency. Ibrahim and Ali [14] investigated these methods and concluded that tuning the resonant frequency is a more efficient technique for applications with a single dominant frequency; whereas methods for widening the frequency bandwidth, including an array of harvesters with different resonant frequencies, multimodal energy harvesting, frequency up-conversion, and nonlinear oscillators [15] are more suitable for multiple frequencies or random vibration sources. Railway bridge vibration falls into the first type with a dominant frequency mainly determined by the dynamic behaviour of the structure, the train configuration, and the travelling speed, although is also affected by uncertainties related to the vehicle–track–structure interaction.

One solution for detuning is the use of self-tuning methods, which are used to increase the frequency bandwidth of optimal performance. For example, Eichhorn et al. [16] proposed a prestressed cantilever piezoelectric energy harvester to adjust the tuning frequency in the interval 440–460 Hz by modifying the tensile preload. The harvester performance could then be improved in environments with shifting vibration frequencies. Similarly, Cheng et al. [17] developed a self-tuning energy harvester by applying an adjustable axial force with a piezoelectric actuator. The simulations showed the self-tuning system increased the output power around 26 times compared to a device with a fixed tuning frequency. Al-Ashtari et al. [18] modified the stiffness of the harvester using two permanent magnets to improve performance in a wide range of excitation frequencies. Furthermore, Karadag et al. [19] proposed a self-tuning method with a movable mass attached to the beam substructure. The proposed tuning algorithm increased the frequency bandwidth to 10%. Also, Kouritem et al. [20] investigated a sliding mass harvesting device to increase the frequency bandwidth. Previous investigations have demonstrated the relevance of adequate resonant frequency tuning on the system output power.

The above concepts can be applied to create optimal designs of harvesters on railway bridges to maximise performance. Energy harvesting on railway bridges is closely related to the dynamic behaviour of the structure and the load induced by trains [21–24]. Typically, a harvester device is tuned to one of the natural frequencies of the hosting structure. However, the bridge behaviour in forced vibration varies due to, among others, the train mass, the travelling speed and the vehicle–bridge interaction, resulting in a shift of the dominant frequencies [25]. Consequently, the performance of a device tuned to the fundamental frequency is suboptimal [21]. Therefore, tuning harvesters for railway bridge applications should not be performed at the bridge natural frequency, but instead should consider changes in the dynamic response during train passage to achieve optimal performance.

The aim of this paper is to investigate the influence of excitation uncertainties on the determination of the optimal tuning frequency in real energy harvesting systems. By isolating and investigating the excitation uncertainties, we intend to address a practical concern in energy harvesting applications and provide specific insights into how these uncertainties affect performance under operating conditions. In this regard, this paper attempts to optimise the frequency tuning of energy harvesters on railway bridges for their implementation in autonomous monitoring systems.

A novel tuning strategy based on a statistical analysis of the bridge response during train passage is proposed. The mechanical energy generated by a lumped-mass model is used as an estimation of the efficiency in converting bridge vibrations into energy. The tuning procedure is divided into three steps: (*i*) experimental measurement of bridge response under different train passages; (*ii*) estimation of the optimal tuning frequency by stochastic analysis of the mechanical energy harvested by tuned lumped-mass systems in a frequency range of interest; and (*iii*) validation under laboratory and operating conditions. This approach is advantageous because it allows for the identification of the optimal tuning frequency without a dynamic identification, thus eliminating the need of complex experimental tests to determine mode shapes and natural frequencies [26,27]. The capabilities of the proposed method are shown through the identification of the most appropriate tuning frequencies on railway bridges on an in-service high-speed line.

The paper is divided into the following parts: Section 2 is concerned with the stochastic analysis of bridge vibrations due to railway traffic and the optimal tuning procedure; the proposed approach is later verified in Section 3; and the results of a real application in a case study are presented Section 4, including bridge modal identification, tuning frequency estimation, design and manufacture of energy harvesters, and energy assessment under operational conditions.

2. Optimal tuning in railway bridges

This section describes the process used for tuning an energy harvester for efficient operation on a railway bridge. First, consider an energy harvester attached to the bridge at a location defined by the coordinate x_b (see Fig. 1). This device is subjected to vertical vibration $z_b(x_b, t)$ induced by a train that travels at a speed V.

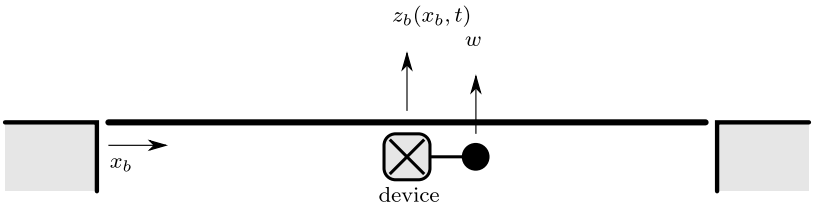

Fig. 1. Scheme of bridge/harvester system.

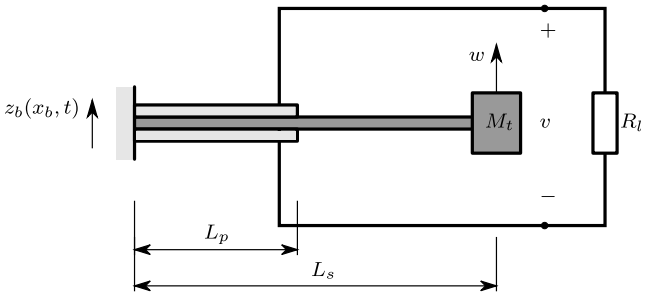

Fig. 2. Scheme of harvester system.

The harvester configuration is a bimorph cantilever beam with a tip mass M_t and two piezoelectric plates (PZT) of length L_p perfectly attached to the substructure (see Fig. 2). The piezoelectrics are polarised in opposite directions along the thickness of the plate and connected in series. The system feeds a load resistance R_l. The geometry of the substructure given by the thickness h_s and length L_s, and the tip mass M_t are selected as the design parameters to adjust the harvester natural frequency to the tuning frequency once the piezoelectric and the substructure material properties have been defined.

In order to estimate the efficiency in the conversion of energy from bridge vibration, a mechanical system is used [28] in this paper for tuning an energy harvesting system. Although the harvester resonant frequency is affected by the electromechanical coupling, and therefore the performance, the authors concluded in Ref. [25] that the influence in devices tuned to low frequencies is very small.

Thus, for simulation purposes, a lumped-mass model is used to represent the dynamic behaviour of the harvester. The properties of the system are given by the lumped mass m, the damping coefficient c and the stiffness k [21]. The mechanical energy in the system during the period T is a function of the velocity of the vibration:

$$E = c \int_0^T |\dot{w}(t)|^2 \, dt \tag{1}$$

where $w(t)$ denotes the vertical displacement of the lumped mass and the damping coefficient c is used to represent the vibration energy transfer from the bridge to the harvester. The instantaneous power then corresponds to the power absorbed by the harvester plus the kinetic energy.

The previous equation can be expressed in terms of the Fourier transform of the harvester velocity according to Parseval's theorem [21]. Then, the displacement of the harvesting device is expressed as:

$$w(\overline{\omega}) = m\overline{\omega}^2 H(\beta) z_b(x_b, \overline{\omega}) \tag{2}$$

where $H(\beta)$ is the frequency response function of the harvester:

$$H(\beta) = \frac{1}{k}\left[\frac{1}{(1-\beta^2) + 2\imath\zeta\beta}\right] \tag{3}$$

where $\beta = \overline{\omega}/\omega$ defines the relation between the loading frequency $\overline{\omega}$ and the natural frequency ω of the lumped mass model, ζ is the damping coefficient and the imaginary unit number is denoted by the Greek letter $\imath$. The natural frequency corresponds to the tuning frequency. Thus, the energy collected becomes:

$$E = \frac{c}{2\pi} \int_{-\infty}^{\infty} \left|\imath\overline{\omega} m \overline{\omega}^2 H(\beta) z_b(x_b, \overline{\omega})\right|^2 d\overline{\omega} \tag{4}$$

The energy harvester's performance is closely related to the dynamic behaviour of the bridge during train passage [21], and maximum harvested energy is obtained when the device is tuned to the fundamental frequency of the bridge [27]. However, the performance of the energy harvester is limited to a narrow frequency bandwidth around the tuning frequency, and therefore the harvested energy is drastically reduced as a result of detuning or deviation from the resonant condition. Although the harvester can

be tuned to the fundamental frequency of the bridge, uncertainties in the dynamic response affect not only the vibration amplitude but also frequency content, thus making the choice of the tuning frequency more difficult.

The dynamic response of a bridge under the passage of a train is affected by several factors. Some are relatively constant such as the bridge properties, while others vary, such as the configuration of train axle spacings, and train speed. Furthermore, some factors and their effect on the bridge are challenging to determine [29], such as structural damping and various interaction mechanisms, the most relevant being vehicle–structure, track–structure, and soil–structure interaction effects. An effective approach is to use stochastic processes to represent the inherent randomness of the generation mechanisms (unevenness, axle loads, train speed, interaction effects, etc.). Thus, the load can be described by a Poisson process [30].

Energy harvesting on railway bridges is then influenced by the uncertainty in the generation mechanisms. Based on the randomness of the bridge vibration, energy harvesting is a stochastic process $\{E(\omega,t_r) : \omega \in \Omega, t_r \in T_r\}$, where $E(\omega,t_r)$ refers to the energy harvested for the train passage t_r in a set of T_r train passages, and Ω denotes the frequency interval of interest in which the harvester can be tuned. The energy distribution is positive and often has an asymmetric distribution with a higher density on the left side of the mean value. Although Gaussian processes are commonly used due to their continuous nature, well-understood properties, and may be sufficient for systems with symmetric data distributions, energy harvesting would require an asymmetric distribution.

The efficiency of statistical inference will be improved by identifying an appropriate distribution to use in modelling train-induced vibration and energy harvesting. Thus, Lombaert et al. [31] presented a methodology to quantify uncertainties in ground-borne vibration using a chi-square distribution with a single degree of freedom. The proposed statistical characteristics of the response were verified for the passage of a TGVA at a speed of 200 km/h and an AGC TER commuter train at a speed of 150 km/h. Daqaq [32] and Gaidai et al. [33] represented the average power of piezoelectric galloping energy harvesters using a Weibull distribution. The shape and mean of the distribution were controlled by the shape and scale parameters. There are also extensions of existing classical distributions to obtain more flexibility and adaptability in data modelling [34], leading to gamma-normal, gamma-Weibull or generalised gamma distributions.

Among these distributions, this paper assumes that energy harvesting in railway bridges can be modelled as a gamma distribution $\{E(\omega,t_r)\} \sim \mathrm{Ga}(a(\omega),b(\omega))$, with the shape and rate parameters $a(\omega)$ and $b(\omega)$ given by [35]:

$$a(\omega) = \frac{b(\omega)}{T_r} \sum_{t_r \in T_r} \left(E(\omega,t_r)\right) \tag{5}$$

$$\frac{1}{b(\omega)} = \frac{1}{T_r^2}\left[T_r \sum_{t_r \in T_r} \left(E(\omega,t_r)\log(E(\omega,t_r))\right) - \sum_{t_r \in T_r} \left(E(\omega,t_r)\right) \sum_{t_r \in T_r} \left(\log(E(\omega,t_r))\right)\right] \tag{6}$$

The gamma distribution is a two-parameter distribution suitable for modelling continuous random processes with positive variables and asymmetric shapes. The gamma distribution, defined by the shape and rate parameters, represents the time required to obtain $a(\omega)$ events in a Poisson process with rate $b(\omega)$. Thus, the gamma distribution can be used to represent the number of train passages required to accumulate an amount of energy, assuming that energy harvesting occurs in discrete events associated with train passages. The energy harvested in each train passage occurs randomly, but on average at a constant rate, and the passage frequency can then be modelled by an exponential distribution. However, instead of considering the time between train passages, the gamma distribution allows us to model the train passages required to accumulate a given amount of energy.

Therefore, the shape parameter $a(\omega)$ defines the energy harvested in $b(\omega)$ train passages. The gamma distribution models the energy harvested in a time window that defines a harvest rate per train passage. The gamma distribution can then be used to analyse the probability that an amount of energy will be accumulated in a period of time, and also to estimate the total time required to achieve the desired energy level. This is useful for the planning and design of energy harvesting systems on railway bridges, as it provides information on the variability of the time required to achieve energy harvesting targets.

Hence, the mean energy $\overline{E}(\omega)$ harvested by a system tuned to the frequency ω during T_r train passages is obtained from Eq. (5) in terms of the shape and rate parameters:

$$\overline{E}(\omega) = \frac{1}{T_r} \sum_{t_r \in T_r} E(\omega,t_r) = \frac{a(\omega)}{b(\omega)} \tag{7}$$

Furthermore, the probability density function (PDF) and cumulative distribution function (CDF) are given by:

$$g(x;a(\omega),b(\omega)) = \frac{b(\omega)^{a(\omega)}}{\Gamma(a(\omega))} x^{a(\omega)-1} e^{-xb(\omega)}, \quad x \geq 0 \tag{8}$$

$$G(x;a(\omega),b(\omega)) = \frac{1}{\Gamma(a(\omega))} \gamma\left(a(\omega), xb(\omega)\right) \tag{9}$$

where x is an estimator of $\{E(\omega,t_r)\}$, $\Gamma(a(\omega))$ is the gamma function and $\gamma(a(\omega),xb(\omega))$ is the incomplete gamma function given, respectively, by [36]:

$$\Gamma(a(\omega)) = \int_0^{\infty} t^{a(\omega)-1} e^{-t}\, dt \tag{10}$$

$$\gamma\left(a(\omega), xb(\omega)\right) = \int_0^{xb(\omega)} t^{a(\omega)-1} e^{-t}\, dt \tag{11}$$

Thus, the confidence interval $CI(\omega;\mathcal{P}) = G(x;a(\omega),b(\omega)) \leq \mathcal{P}$ defines the energy harvested by a system tuned to the frequency ω during T_r train passages with a confidence level $\mathcal{P}$. In [21,25] it was shown that the harvested energy reaches the highest levels when the device is tuned around the fundamental frequency of the bridge. Therefore, the confidence interval presents a global or local maximum at the frequencies $\widehat{\omega}$ around a natural frequency of the bridge given by the following:

$$\max\{CI(\omega;\mathcal{P})\} = CI(\widehat{\omega};\mathcal{P}), \quad \omega \in \Omega \tag{12}$$

In addition, the energy harvested by a device tuned in the frequency interval $\mathcal{E}_{\Delta\widehat{\omega}}(\widehat{\omega}) = [\widehat{\omega}-\Delta\widehat{\omega}, \widehat{\omega}+\Delta\widehat{\omega}]$ presents a maximum peak for each train passage $tr \in Tr$ at frequency $\omega^*(tr)$, which can also be described as a random process $\{\omega^*(tr) : \omega^*(tr) \in \mathcal{E}_{\Delta\widehat{\omega}}(\widehat{\omega}), tr \in Tr\}$ that follows a Gaussian distribution $N(\widehat{\mu},\widehat{\sigma})$. Moreover, the accumulated energy harvested by a device tuned to the mean frequency $\widehat{\mu}$ of the distribution is maximised in the interval $\mathcal{E}_{\Delta\widehat{\omega}}(\widehat{\omega})$ for train passages $tr \in Tr$, as will be shown later.

Therefore, the optimal tuning frequency corresponds to the mean of the distribution $N(\widehat{\mu},\widehat{\sigma})$, i.e. $\omega_t = \widehat{\mu}$. The tuning frequency represents the most probable frequency excited by train passages. Thus, the overall energy harvested by a device tuned to ω_t is maximised.

2.1. Tuning procedure

The tuning process is subdivided into four steps: (*i*) experimental measurement of the bridge response due to railway traffic; (*ii*) computation of mechanical energy for train passages $tr \in Tr$ and harvesters tuned in the frequency range of interest $\omega \in \Omega$; (*iii*) statistical characterisation of the energy distribution $\{E(\omega,tr)\} \sim \text{Ga}(a(\omega),b(\omega))$; and (*iv*) estimation of the tuning frequency ω_t according to the approach previously presented.

A key issue in the tuning process is the definition of the tuning interval $\mathcal{E}_{\Delta\widehat{\omega}}(\widehat{\omega})$, which must ensure the peak energy frequency distribution follows a normal distribution $N(\widehat{\mu},\widehat{\sigma})$. For this purpose, two conditions are imposed: (*i*) the one-sample Kolmogorov–Smirnov test [37] must satisfy the null hypothesis that the peak energy frequency comes from a normal distribution; and (*ii*) the quantile–quantile representation must fit the input sample $\omega^*(tr)$ with a coefficient $R^2 \geq 0.9$. The quantile–quantile plot represents the quantile of the input sample $\omega^*(tr)$ against the theoretical values given by the normal distribution. The quantiles q_{tr} of the sample are computed at midpoints of equally spaced intervals using cumulative probabilities from 0 to 1:

$$p_{tr} = \frac{tr-0.5}{N_{tr}}, \quad tr = 1,2,\dots,N_{tr}, \quad tr \in Tr \tag{13}$$

where N_{tr} is the number of train passages used in the tuning procedure. The quantile of the input sample corresponds to the sorted values of $\omega^*(tr)$. The theoretical quantile $\overline{q}_{tr}$ of the normal distribution is computed from the inverse of the CDF as:

$$\overline{q}_{tr} = \widehat{\mu} + \widehat{\sigma}\sqrt{2}\text{erf}^{-1}(2p_{tr}-1) \tag{14}$$

where $\text{erf}(p)$ is the error function.

Then, the coefficient of determination R^2 is obtained from the linear regression of quantiles of the input sample $\omega^*(tr)$ using the lower and upper theoretical quartiles of the normal distribution corresponding to 25% and 75% percentiles:

$$R^2 = 1 - \frac{SS_{\text{Res}}}{SS_{\text{Tot}}} = 1 - \frac{\sum_{tr=1}^{N_{tr}}(q_{tr}-\overline{q}_{tr})^2}{\sum_{tr=1}^{N_{tr}}(q_{tr}-\widehat{\mu})^2} \tag{15}$$

where SS_{Res} and SS_{Tot} represent the residual and the total sum of squares, respectively.

Table 1 summarises the tuning procedure. The optimum tuning frequency is characteristic of each bridge, as it depends on the dynamic properties of the structure and the operating conditions, as will be discussed below. The experimental assessment of the bridge response due to railway traffic (task *A* in Table 1) can be performed with a portable system (e.g. laser vibrometer) at a single measurement point. Although a larger number of measurement points can lead to a better knowledge of the dynamic behaviour of the bridge (mode shapes, natural frequencies and modal damping), a single point is sufficient to estimate the tuning frequency if the location is appropriately chosen to assess the contribution of the first mode shapes. Simultaneous measurement at multiple points would require at least one reference or a sufficient number of sensors for cross-correlation of the bridge response, which would increase the cost of the test. The proposed method is intended to be cost-effective as it uses a single non-contact measurement and is advantageous as it does not require modal identification of the structure and avoids the effort associated with an experimental analysis test.

3. Verification

The proposed tuning procedure is verified from the experimental records of a bridge in the Spanish Madrid-Sevilla high-speed line (Fig. 3). The proposed method is verified by comparing the natural frequency related to the fundamental mode shape with the statistical characterisation $\omega^*(Tr) \sim N(\widehat{\mu},\widehat{\sigma})$ of the frequency peak energy $\omega^*(tr)$ in $\mathcal{E}_{\Delta\widehat{\omega}}(\widehat{\omega})$, and the tuning frequency estimated as $\omega_t = \widehat{\mu}$. The fundamental mode shape corresponded to the first longitudinal bending mode at the natural frequency $f_{b1} = 6.3\,\text{Hz}$. The modal parameters and the dynamic behaviour of the bridge under operational conditions can be found in Ref. [27].

In this paper, the bridge responses due to train passages are used to determine the optimum tuning frequency that is corroborated by the identified natural frequency. This analysis allows for the verification of the assumptions stated in the previous section related to the statistical characterisation of the mechanical energy and its application in determining the optimum tuning frequency. In the

Table 1
Summary of tuning procedure.

A *Experimental measurement of bridge response due to railway traffic.*
B *Assessment of mechanical energy.*
B.1 Definition of the tuning frequency range of interest $\omega \in \Omega$.
B.2 Computation of mechanical energy for train passages $tr \in Tr$.
C *Stochastic analysis of mechanical energy.*
C.1 Statistical characterisation of mechanical energy $\{E(\omega, tr)\} \sim \text{Ga}(a(\omega), b(\omega))$.
C.2 Identification of confidence interval CI and maximum energy frequencies $\widehat{\omega}$.
D *Estimation of the tuning frequency.*
D.1 Set frequency interval $\mathcal{E}_{\Delta\widehat{\omega}}(\widehat{\omega})$ around $\widehat{\omega}$.
D.2 Find maximum energy peak frequency for each train passage $\omega^*(tr)$ in $\mathcal{E}_{\Delta\widehat{\omega}}(\widehat{\omega})$.
D.3 Statistical characterisation of $\omega^*(Tr) \sim N(\widehat{\mu}, \widehat{\sigma})$.
D.4 Check the one-sample Kolmogorov–Smirnov test of the sample $\omega^*(Tr)$.
D.5 Check the determination coefficient R^2 of the quantile–quantile representation of the input sample $\omega^*(Tr)$.
D.6 If the above is fulfilled, then the tuning frequency is estimated as $\omega_t = \widehat{\mu}$.

Fig. 3. HSL bridge over Jabalón river (38°53′51.3″N 3°57′53.0″W).

following section, the proposed method is used to blindly (without knowledge of the modal parameters) tune harvesters at different natural frequencies.

Twenty train passages were recorded, all of which were RENFE high-speed services travelling at velocities between $V = 236$ km/h and $V = 290$ km/h. Fig. 4 shows the time history of bridge acceleration at measurement point $A2$ (see Ref. [27]) induced by three different trains: a Renfe S102 travelling at $V = 290$ km/h (passage #1), a Renfe S012 at $V = 240$ km/h (passage #5), and a Renfe S100 at $V = 290$ km/h (passage #17). Additional information on the train configurations and axle distances can be found in [27].

The mechanical energy in Fig. 4 was calculated from Eq. (4) for harvesters tuned in the frequency range 1−10 Hz, considering a damping ratio $\zeta = 1\%$. The damping coefficient is calculated as $c = 2\zeta\sqrt{km} = 0.09$ N s/m using a relation $r = km = 20$ kg N/m to obtain a comparable analysis of energy harvested over the frequency range [21]. Then, the lumped mass and the stiffness were calculated from the tuning frequency as $m = c/(2\zeta\omega)$ and $k = \omega c/(2\zeta)$. The distribution of peak energy for each train passage in Fig. 4.(d–f) shows clear frequency dispersion at: $f^*(1) = 5.6$ Hz, $f^*(5) = 4.9$ Hz and $f^*(17) = 5.9$ Hz; in each case ($\omega^*(tr) = 2\pi f^*(tr)$).

The statistical characterisation of the energy distribution showed a maximum at the tuning frequency $\widehat{f} = 5.6$ Hz ($\widehat{\omega} = 2\pi\widehat{f}$) as can be seen in Fig. 5.(a). The CI corresponded to a confidence level of 97%. The one-sample Kolmogorov–Smirnov test satisfied the null hypothesis in the interval $\mathcal{E}_{0.3}(5.6)$ (shaded in grey) at the significance level of 1% with a $p-$ value equal to 0.54. Thus, the sample was normally distributed with $N(5.7, 0.1)$ (expressed in Hz). The quantile–quantile plot (Fig. 5.(b)) shows a good correlation between the peak energy frequency $f^*(tr)$ for each train passage (input sample) and the theoretical quantiles of the normal distribution. The determination coefficient was $R^2 \geq 0.93$.

Then, the tuning frequency can then be estimated as the mean value of the distribution $f_t = 5.7$ Hz. This shows the tuning frequency is lower than the natural frequency $f_{b1} = 6.3$ Hz of the fundamental mode identified from the ambient vibration. Although the natural frequency of the bridge was known in this analysis, it is not necessary to calculate the tuning frequency. The following section shows the results of a case study on an HSL railway bridge.

4. Case study

This section reports the design, tuning, and in-field validation of two energy harvesters on a HSL railway bridge. An experimental program is carried out to determine the optimal tuning frequency, the modal identification, and the energy assessment under operational conditions. The design, manufacture, and performance of the energy harvesters are presented. Moreover, the energy loss due to detuning is analysed to validate the tuning process.

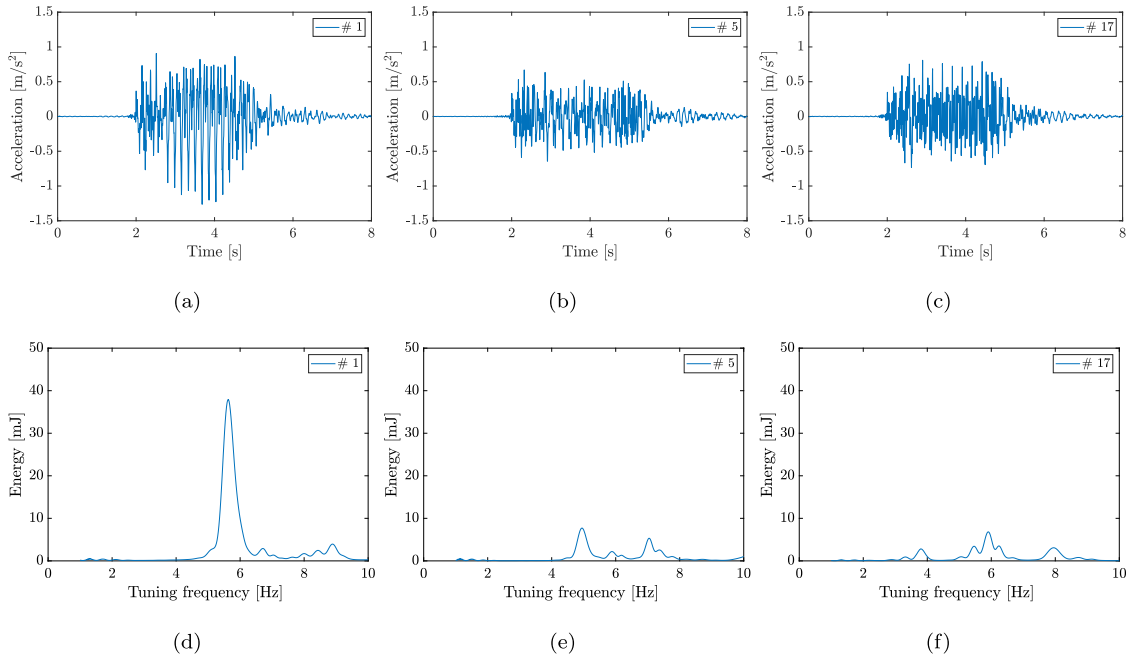

Fig. 4. (a,b,c) Time history of bridge acceleration and (d,e,f) mechanical energy harvested for train passages #1, #5 and #17.

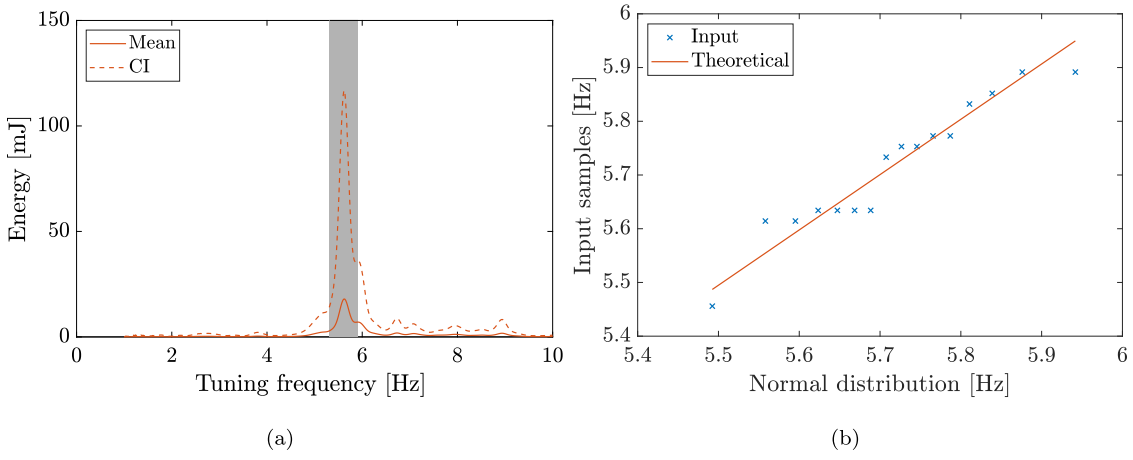

Fig. 5. (a) Energy distribution and (b) quantile–quantile plot for $\hat{f} = 5.6$ Hz.

4.1. Experimental program

A second experimental program was carried out on a HSL bridge crossing the Tirteafuera river in July and September 2022. It was a single simply-supported span concrete bridge with three tracks (see Fig. 6). The deck was composed of a 18 m × 20.6 m (length × width) concrete slab resting on ten prestressed concrete girders. The slab carried two ballasted tracks with UIC gauge (1.435 m) for high-speed trains and one ballasted track with Iberian gauge (1.668 m) for conventional traffic.

The tests were carried out in two stages. First, the bridge response due to railway traffic was measured with a laser vibrometer. This allowed for the identification of the optimal tuning frequency according to Table 1 and thus the manufacturing requirements of the harvesters. Next, the proposed procedure was validated experimentally using a comprehensive experimental campaign consisting of the measurement of the bridge response from both ambient and forced vibrations. Fig. 7 shows the sensors layout on the deck. The results of the second test include the identification of the bridge modal properties and the energy harvested under operating conditions.

The experimental setup (Fig. 8) consisted of an Ometron VH-1000-D laser vibrometer with sensitivity 8.0064 V/m/s and piezoelectric accelerometers with a nominal sensitivity of 10 V/g. The laser vibrometer was used in the first test to record the

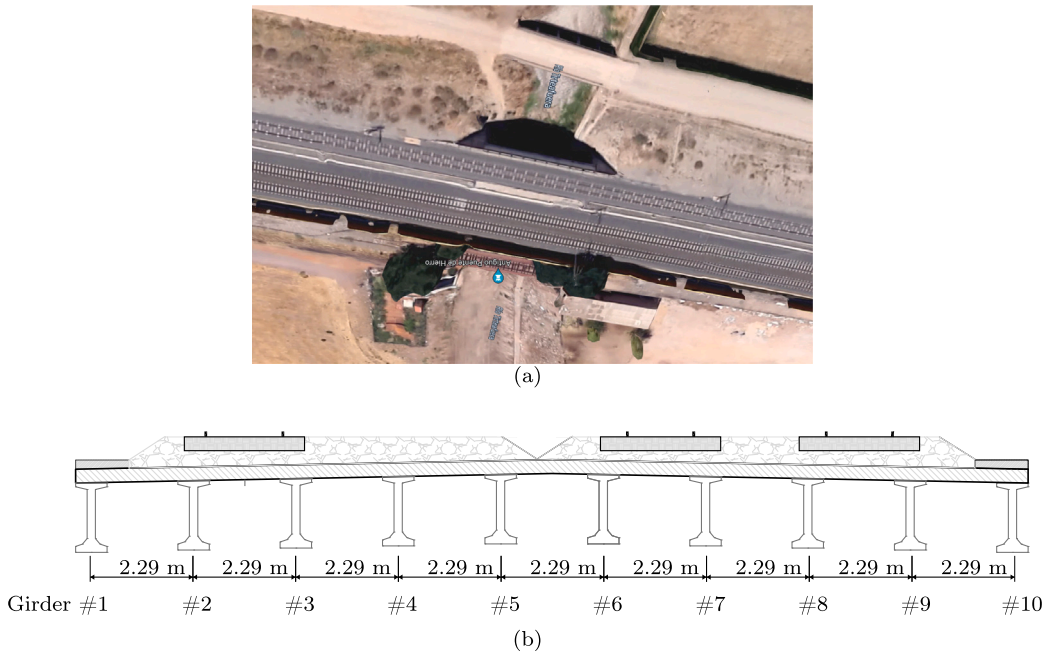

Fig. 6. HSL bridge under study: (a) general view (38°43′33.06″N 4°5′20.05″W) and (b) cross section.

vibrations produced by railway traffic (Fig. 8.(c)), avoiding the installation of the complex scaffolding system in Fig. 8.(d). The laser vibrometer was also used in the second test to measure the harvester response. The bridge response was recorded using piezoelectric accelerometers. The Analog/Digital (A/D) conversion was performed with a LAN-XI portable acquisition system from Brüel & Kjaer. A/D was performed at a sampling frequency of 512 Hz, which avoided aliasing effects. The response was filtered by applying a 1 Hz high-pass third-order Chebyshev filter.

The test setup initially included 24 measurement points ($A1-A24$) evenly distributed on the bridge. However, the number of points was reduced to 11 due to the difficulty in installing the scaffolding system due to the poor condition of the ground below the bridge. The discarded points are represented in grey in Fig. 7.

4.2. Tuning frequency estimation and bridge modal identification

The dynamic response of railway bridges composed of simply supported spans is generally dominated by the contribution of modes below 30 Hz, corresponding to the first longitudinal bending, torsional and transverse bending modes. Maximum modal amplitudes are found at the mid-span and at the deck edge [38–40]. The bridge considered in this article is approximately square in plan and the contribution of mode shapes can be significant in these modes. The response of the bridge at measurement point $A14$ (Fig. 7) was used in the first stage to estimate the tuning frequency. This point was chosen in the middle of the span, but slightly offset towards the deck edge in order to assess the contribution of the above mode shapes. A total of 19 train circulations were recorded on July 5th 2022 between 10:00 and 13:00 h. Table 2 summarises the train passages, including train type, track number, and speed.

Fig. 9 shows the bridge response and mechanical energy estimated for different train passages. The mechanical energy was estimated for harvesters tuned in the frequency range 1–15 Hz with a damping ratio of $\zeta = 1\%$. The three train passages represented in Fig. 9 were: Renfe S102 travelling at $V = 183.1$ km/h (passage #1), Renfe S103 at $V = 231.8$ km/h (passage #10) and Renfe S102 at $V = 224.5$ km/h (passage #16). The peak energy for each passage was obtained at the tuning frequencies $f^*(1) = 7.9$ Hz, $f^*(10) = 7.2$ Hz and $f^*(16) = 9.3$ Hz. Similar dispersion in peak energy frequency was also observed all other train passages.

The statistical characterisation of the mechanical energy obtained from the total train circulations is represented in Fig. 10.(a). The confidence interval of the energy distribution reached maximum levels at approximately 2.5 Hz, 7.8 Hz, and 9.3 Hz. The first frequency corresponds to the bogie passage frequency, which depends on the train configuration and the moving speed. The second and third frequencies corresponded to the natural frequencies of the bridge with slight deviations, as was later verified from the modal identification in the second stage. It should be noted that this correspondence was not known at this stage, but the energy distribution around these values was indicative of resonant frequencies in the bridge response. Moreover, it was assumed that in the first case, the mode shape could be the first longitudinal bending mode shape and, in the second case, the first torsional or transverse bending mode shapes. These assumptions were based on the typical dynamic bridge behaviour identified in the past by the authors on similar typologies [27] and were later verified using modal identification.

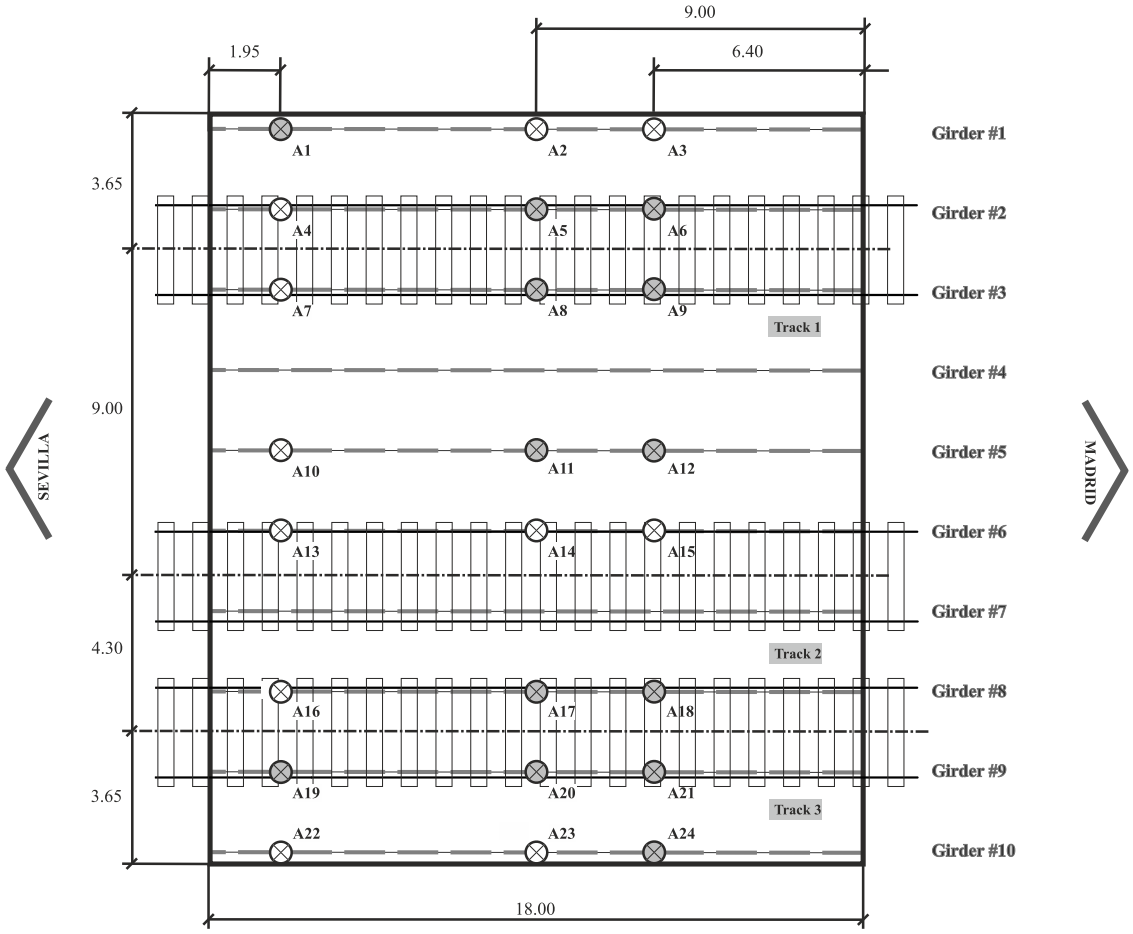

Fig. 7. Sensor layout.

Table 2
Summary of train passages in the first experimental stage.

Passage	Train	Track	V [km/h]
1	S102	2	183.1
2	S102	3	200.6
3	S100	2	177.6
4	S114	2	221.0
5	S114	2	232.2
6	S103+S102-duplex	3-2	191.2
7	S114	3	197.7
8	S120	2	220.0
9	S120	3	220.0
10	S103	3	231.8
11	S100	2	168.6
12	R449	1	159.1
13	S114	3	198.0
14	S114	2	220.0
15	S100	3	176.8
16	S102	3	224.5
17	S102-duplex	2	176.4
18	S102	2	183.2
19	S100-duplex	2	184.4

The tuning frequency was estimated from the maximum peak for each circulation in the intervals $\mathcal{E}_1(7.8)$ and $\mathcal{E}_{0.5}(9.3)$ around the maximum in the confidence intervals found at $\widehat{f_1} = 7.8$ Hz and $\widehat{f_2} = 9.3$ Hz (shaded in grey). The peak energy frequencies in the selected intervals were characterised by a normal distribution given by $N_1(7.9, 0.4)$ and $N_2(9.3, 0.2)$ (in Hz). The Kolmogorov–Smirnov

Fig. 8. Experimental setup: (a) transducer view, (b) energy harvester and accelerometer, (c) laser vibrometer, and (d) scaffolding system.

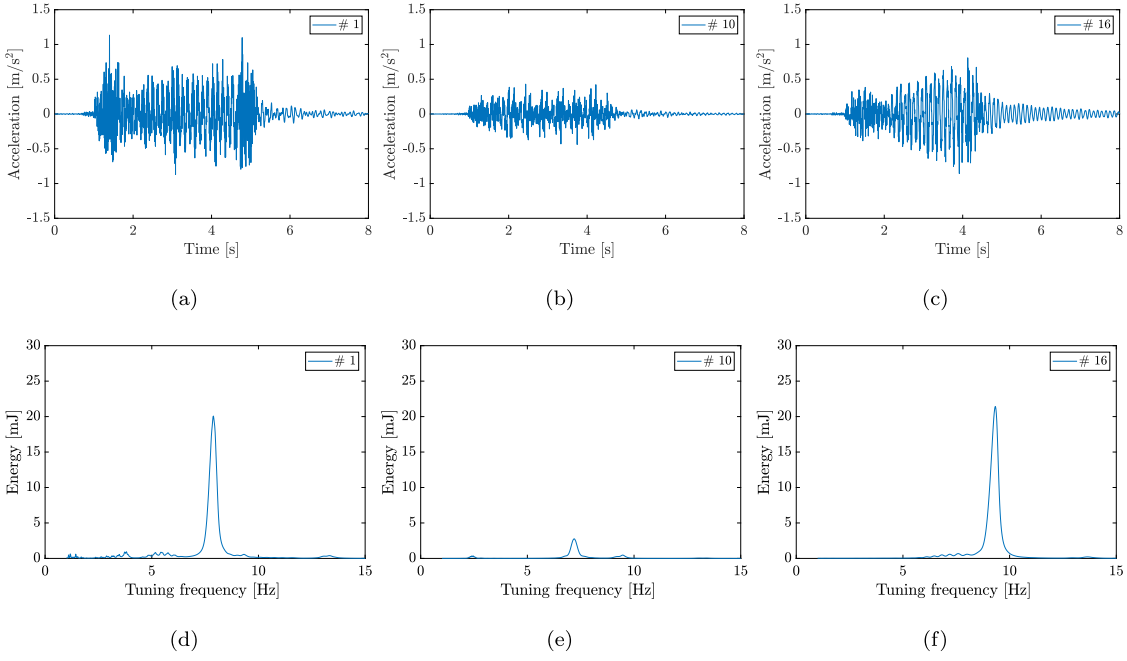

Fig. 9. (a,b,c) Time history of bridge acceleration and (d,e,f) mechanical energy harvested for different train passages (see Table 2).

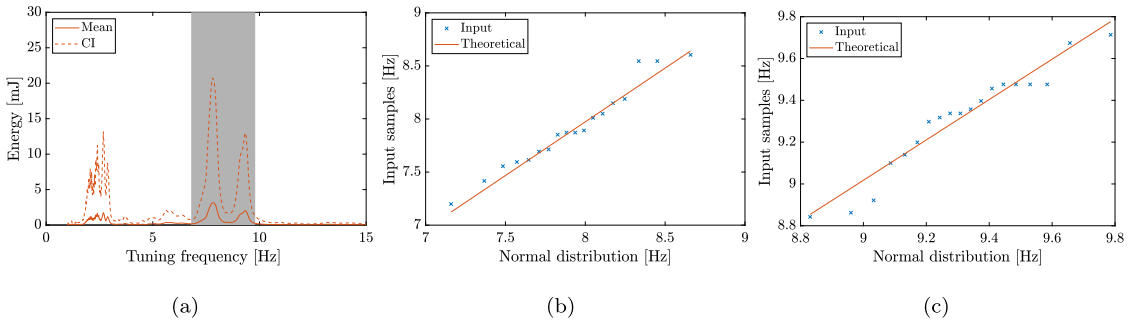

Fig. 10. (a) Energy distribution and quantile–quantile plots for (b) $\hat{f} = 7.8\,\text{Hz}$ and (c) $\hat{f} = 9.3\,\text{Hz}$ in the HSL bridge under study.

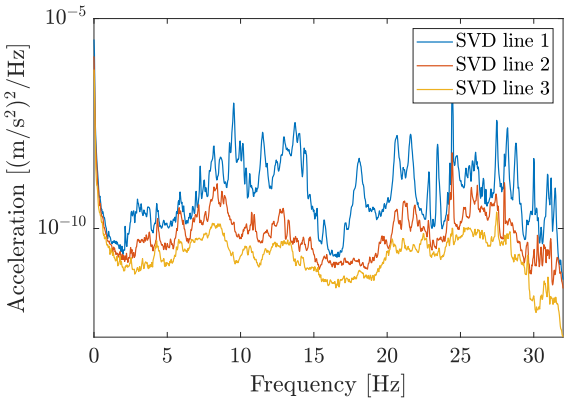

Fig. 11. Singular value decomposition.

test satisfied the null hypothesis in both cases with $p-$ values equal to 0.89 and 0.60, respectively. The quantile–quantile plots show the peak energy frequencies were found to be in good agreement with the normal distributions. The coefficients were $R_1^2 = 0.96$ and $R_2^2 = 0.94$, respectively. Therefore, the tuning frequencies were obtained from the mean value of the normal distribution in each case as $f_{t1} = 7.9\,\text{Hz}$ and $f_{t2} = 9.3\,\text{Hz}$. The bogie passing frequency was not considered in the tuning procedure due to uncertainties related to the train in service configuration and speed.

Later, from the measurements performed during the second stage of the experimental campaign, the modal parameters of the bridge were identified from ambient vibration through an operational modal analysis (OMA) using the Enhanced Frequency Domain Decomposition (EFDD) [41,42]. Fig. 11 shows the power spectral density of the measured acceleration using the singular value decomposition (SVD). The identified mode shapes, the natural frequencies, and the modal damping were: (*i*) the first longitudinal bending mode shape of the bridge deck with the high-speed track ($f_{b1} = 8.1\,\text{Hz}$, $\zeta_{b1} = 1.7\%$); (*ii*) the first longitudinal bending mode shape of the bridge deck with the conventional track ($f_{b2} = 8.7\,\text{Hz}$, $\zeta_{b2} = 1.4\%$); (*iii*) the first transverse bending mode shape ($f_{b3} = 9.5\,\text{Hz}$, $\zeta_{b3} = 0.5\%$); and (*iv*) the first torsional mode shape ($f_{b4} = 11.5\,\text{Hz}$, $\zeta_{b4} = 0.8\%$) (see Fig. 12). The weak coupling between high-speed and conventional sections of the deck was noticeable, as can be seen in Fig. 12(a,b). The tuning frequencies were related to the first longitudinal and first transverse bending mode shapes of the bridge. The tuning frequency $f_{t1} = 7.9\,\text{Hz}$ was slightly lower than the first natural frequency $f_{b1} = 8.1\,\text{Hz}$. The second tuning frequency $f_{t2} = 9.3\,\text{Hz}$ corresponded to the transverse bending mode shape with natural frequency $f_{b3} = 9.5\,\text{Hz}$. Therefore, the above assumptions related to the correspondence of the tuning frequencies with the mode shapes were verified.

4.3. Design, manufacture and performance verification of energy harvesters

After the tuning frequencies were estimated, two energy harvesters were designed and manufactured following the optimal design procedure proposed in Ref. [25]. The piezoelectric patch selected was the commercial DuraAct patch transducer P-876.A12 [43], composed of a piezoelectric layer covered with copper electrodes. The patch was embedded in a structure mechanically pre-stressed by a polymer surface, providing certain flexibility. The patch dimensions were: length $L_p = 50\,\text{mm}$, width $b_p = 30\,\text{mm}$, and thickness $h_p = 0.2\,\text{mm}$. The properties of the PZT material were: Young's modulus $c_{11}^E = 123\,\text{GPa}$, piezoelectric constant $e_{31} = -7.15\,\text{N/Vm}$, relative permittivity at constant strain $\epsilon_{33}^S = 857\epsilon_0$, where $\epsilon_0 = 8.854 \times 10^{-12}\,\text{F/m}$ is the vacuum permittivity and density $\rho_p = 7800\,\text{kg/m}^3$. The P-876.A12 patch worked in the 31 mode and was polarised along the thickness.

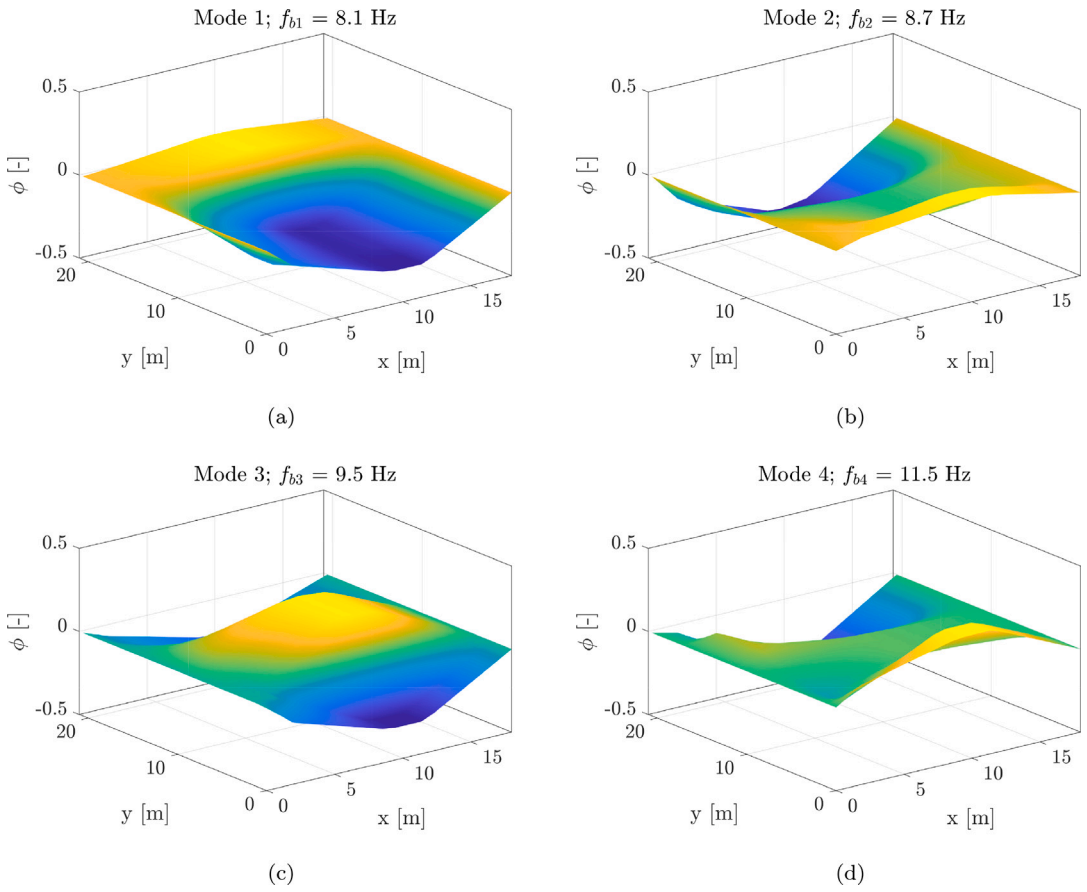

Fig. 12. Identified mode shapes of the bridge under study.

Table 3
Optimal design parameters.

Tuning frequency	L_s [mm]	h_s [mm]	M_t [kg]	R_l [kΩ]
f_{t1} = 7.9 Hz	106.4	0.94	0.09	664
f_{t2} = 9.3 Hz	90.7	0.75	0.08	552

Additive manufacturing using 3D FDM printing was selected for the substructure. A high-temperature resistance polyamide carbon fibre reinforced material (PAHT CF15) [44] was used as an alternative to metal due to its high strength. The material properties were experimentally determined to assess the influence of the printing configuration. Five printed specimens using a special alloy steel hotend with a nozzle of 0.6 mm were tested according to ASTM D638-14 [45]. The infill was set at 100%, the printing temperature to 280 °C with a build plate temperature of 95 °C, and the print and travel speeds to 40 mm/s and 200 mm/s, respectively. The estimated material properties were: mean Young's modulus E_s = 7.40 GPa with a standard deviation of s_E = 0.33 GPa, and tensile strength σ_y = 94 MPa with a standard deviation of s_{σ_y} = 9.9 MPa. The experimentally determined properties were used for the rest of the study.

The devices were designed using an optimal design method [25]. The substructure geometry, tip mass and load resistance that maximised output power were obtained using a genetic algorithm with constraints on geometry and structural integrity. The design parameters were the length and thickness of the substructure, L_s and h_s, and the tip mass M_t. The width of the substructure was considered fixed and equal to the width of the PZT patch. The genetic algorithm started by tuning random individuals to the tuning frequency. The design parameters h_s, L_s and M_t were calculated from the individuals in each generation and the output power was evaluated if the constraints were satisfied. This process was repeated in subsequent generations to find the optimal harvester design.

The results of the optimisation design are summarised in Table 3. The geometry consisted of the substructure, the piezoelectric patches, a clamp to attach the harvester to the bridge, and a hollow cylinder for the tip mass. Fig. 13 shows the printed prototype with the piezoelectric patches glued to the substructure.

The performance of the prototypes was verified in the laboratory by comparing the experimental and analytical frequency response functions for the tip response and the output voltage [25]. The experimental test consisted of measuring the response of the

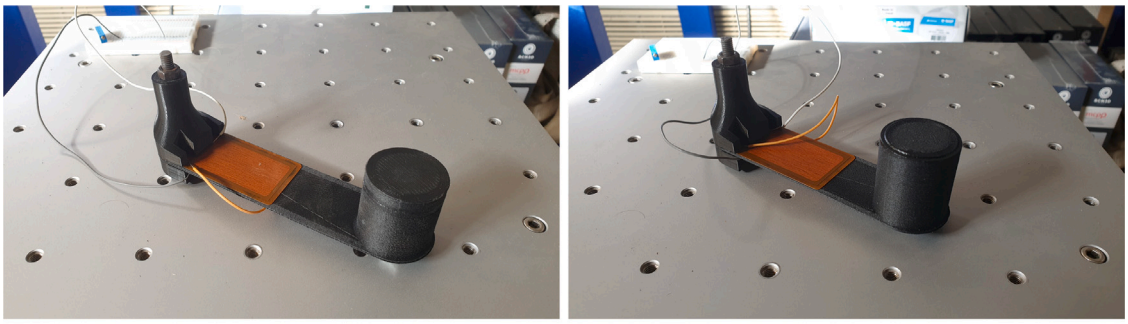

(a) (b)

Fig. 13. Energy harvester prototypes tuned to (a) $f_{t1} = 7.9$ Hz and (b) $f_{t2} = 9.3$ Hz.

Table 4
Damping ratio and electromechanical coupling coefficient.

Tuning frequency	ζ_{Ana} [%]	ζ_{Exp} [%]	α_{Ana} [$\times 10^{-4}$ N/V]	α_{Exp} [$\times 10^{-4}$ N/V]
$f_{t1} = 7.9$ Hz	1.00	1.00	2.20	2.19
$f_{t2} = 9.3$ Hz	1.00	0.96	2.58	2.60

device due to the base excitation induced by an APS 400 ELECTRO-SEIS electrodynamic shaker. The tip velocity was measured using a laser vibrometer, and the output voltage was recorded directly with the acquisition system. Furthermore, the base acceleration was measured with an accelerometer with nominal sensitivity 100 mV/g. The device was subjected to a burst of random acceleration in a 50 Hz bandwidth lasting 128 s. The burst percentage was established at 50% of the total test time.

Fig. 14 shows the experimental Frequency Response Functions (FRF) and the analytical solution [25] for tip acceleration and voltage. The agreement between both sets is strong. The damping coefficient ζ and the electromechanical coupling factor α were investigated by fitting the analytical solution of the FRF to the experimental response. The Levenberg–Marquardt non-linear least squares algorithm [46] was used to fit the frequency response function for tip acceleration and voltage. Table 4 shows the experimental values (ζ_{Exp} and α_{Exp}) and the analytical estimations (ζ_{Ana} and α_{Ana}). The agreement in the results verified the performance of the energy harvesters under laboratory conditions.

4.4. Energy assessment under operational conditions

This section presents the results obtained from the harvesters installed on the in-situ bridge. On September 7th 2022, 18 passenger train circulations were recorded between 15:57 and 18:11 h. All trains were RENFE High-Speed services and one diesel convoy circulating on the conventional line. The energy harvesters tuned to f_{t1} and f_{t2} were located at the measurement points $A14$ and $A23$, respectively (see Fig. 7), where the maximum modal amplitude is reached in each case. Once again, it should be noted that the mode shapes were unknown at this stage.

The selected location for the energy harvesters was chosen on the basis that the dynamic response of railway bridges composed of simply supported spans is generally dominated by the contribution of the first longitudinal, first torsional and first transverse bending modes. The frequency f_{t1} was then assumed to be associated with the first longitudinal bending mode shape, while f_{t2} was associated with the first torsional or transverse bending mode shapes. Maximum amplitudes are found at the mid-span and deck edge for these mode shapes [27], which become the preferred locations for energy harvesting. These hypotheses were confirmed by the identified mode shapes in Fig. 12. Therefore, for slab bridges, the contribution of the first torsional and transverse bending modes, in addition to the first longitudinal bending mode, must be considered in the design of energy harvesting systems.

Table 5 summarises the train passages, speed, and energy generated by the harvesters. The energy levels varied in a wide range depending on the train type and speed. An overall analysis showed that the total energy $E_{t1} = 1.363$ mJ produced by the harvester tuned to $f_{t1} = 7.9$ Hz was lower than $E_{t2} = 6.279$ mJ for the device tuned to $f_{t2} = 9.3$ Hz. The energy harvested from railway traffic in a time window of three hours (18 train passages) was 7.65 mJ. The energy harvested by each device is distributed according to the shape and rate parameters $a(f_{t1}) = 0.62$ mJ and $b(f_{t1}) = 8.16$ trains, and $a(f_{t2}) = 0.26$ mJ and $b(f_{t2}) = 0.75$ trains, respectively. In addition, a comparative analysis to assess the performance of energy harvesting from ambient vibrations resulted in an increase of 0.0025 mJ, which can be considered as residual, approximately 0.03% of the energy harvested during train passages.

The analysis of the energy harvested showed there were train passages of maximum energy such as passage #7 with $E_{t2} = 1.813$ mJ and near zero energy train passages such as passage #9 with $E_{t2} = 0.066$ mJ. The influence of the train configuration and speed on the bridge response is analysed in the following to better understand the differences in the energy levels. It is well known that successive passage of equally spaced loads can cause a resonant behaviour of the bridge when the train speed is close to the resonant velocity $V_{jn}^{r} = f_{bj}d/n$, where j makes reference to the excited natural frequency, n is the number of cycles between loads

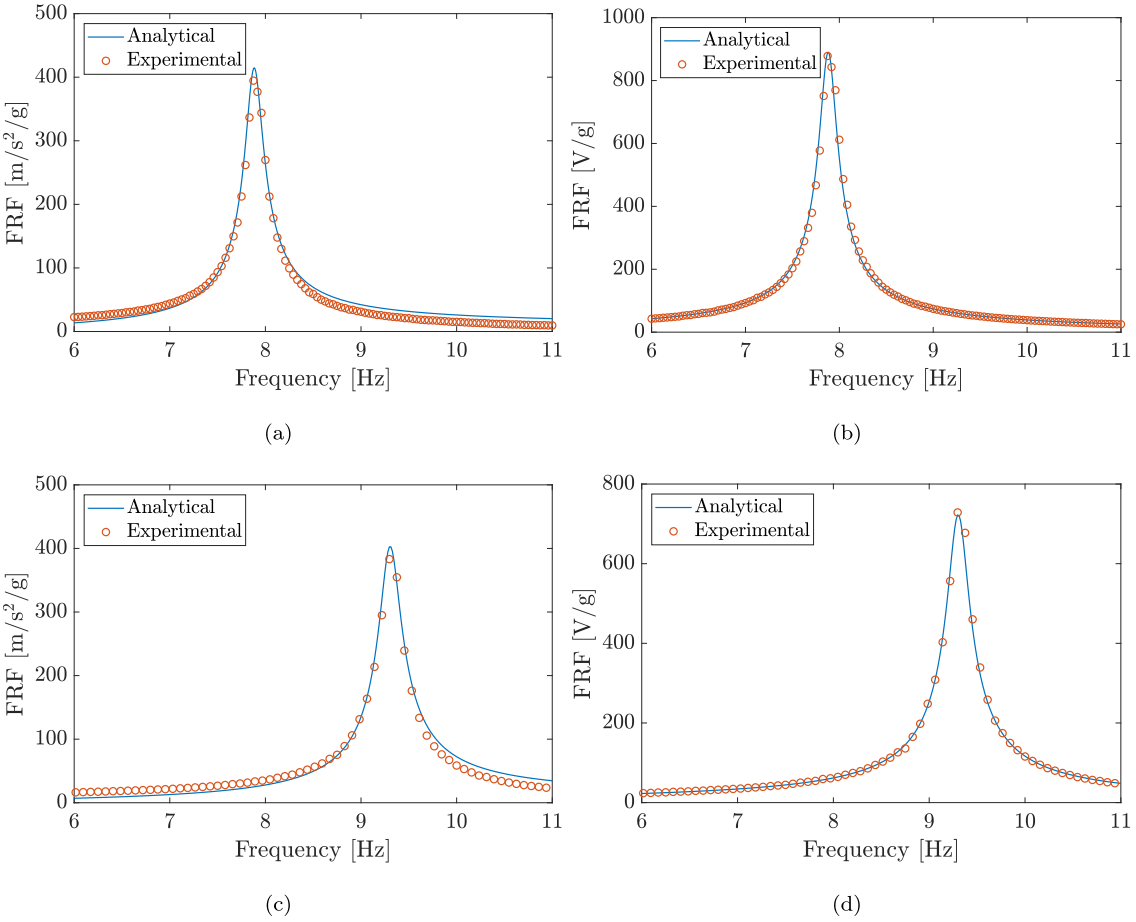

Fig. 14. Analytical and experimental frequency response function of (a,c) tip acceleration and (b,d) voltage of energy harvesters tuned to (a,b) $f_{t1} = 7.9$ Hz and (c,d) $f_{t2} = 9.3$ Hz.

Table 5
Energy harvesting in train passages [mJ] at the bridge under study: in situ test E_{t1} and E_{t2}, analytical estimation for optimal tuning $\overline{E}_{t1}$ and $\overline{E}_{t2}$, and estimation for devices tuned to related bridge resonant frequencies $\overline{E}_{b1}$ and $\overline{E}_{b3}$.

Passage	Train	Track	V [km/h]	E_{t1} [mJ]	E_{t2} [mJ]	$\overline{E}_{t1}$ [mJ]	$\overline{E}_{t2}$ [mJ]	$\overline{E}_{b1}$ [mJ]	$\overline{E}_{b3}$ [mJ]
1	S100	2	178.2	0.046	0.013	0.027	0.006	0.037	0.007
2	S100	3	202.5	0.012	0.009	0.004	0.007	0.009	0.007
3	252	2	149.2	0.030	0.151	0.267	0.116	0.282	0.122
4	S114	3	220.0	0.009	0.005	0.003	0.011	0.008	0.006
5	S102	3	213.8	0.034	1.903	0.025	1.810	0.032	1.462
6	S102	2	177.8	0.544	0.038	0.992	0.063	0.335	0.031
7	S102-duplex	3	210.8	0.071	1.813	0.050	4.329	0.068	1.369
8	S114	2	186.4	0.012	0.005	0.062	0.002	0.014	0.003
9	S103	2	116.0	0.020	0.066	0.021	0.117	0.018	0.057
10	S130	2	180.6	0.178	0.030	0.555	0.016	0.138	0.020
11	S100	3	179.9	0.081	0.005	0.020	0.003	0.057	0.003
12	R598	1	135.8	0.003	0.018	~ 0.0	0.025	~ 0.0	0.021
13	S114	3	213.0	0.011	0.005	0.003	0.006	0.008	0.005
14	S100	2	187.4	0.030	0.008	0.018	0.006	0.020	0.006
15	S100	3	193.6	0.020	0.005	0.008	0.004	0.017	0.003
16	S102	2	176.4	0.180	0.034	0.582	0.035	0.164	0.030
17	S100	2	175.4	0.018	0.022	0.068	0.009	0.016	0.017
18	S102-duplex	3	211.4	0.068	2.147	0.056	5.804	0.070	1.936
			Total	1.363	6.279	2.760	12.369	1.293	5.105

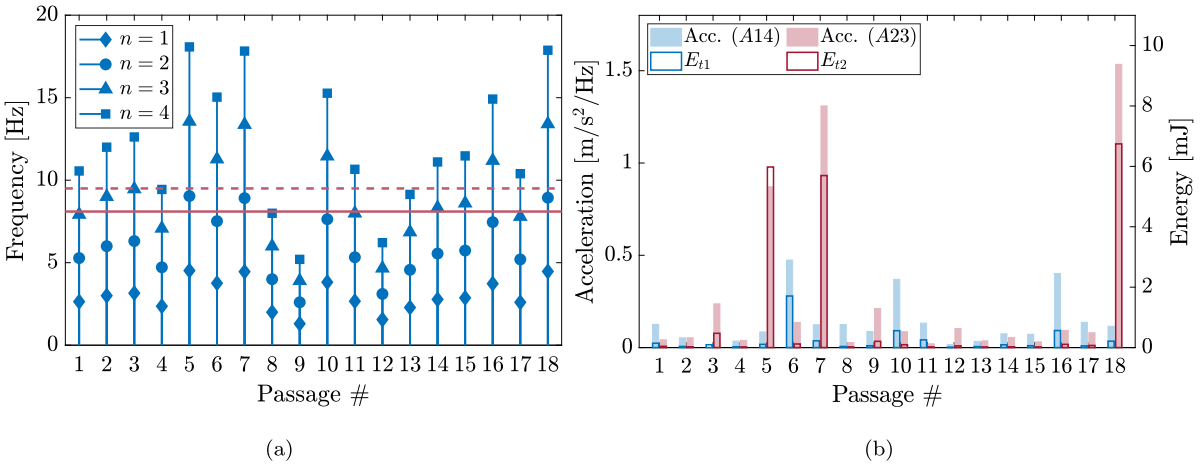

Fig. 15. (a) Bogie passing frequency and its related higher-order harmonics for different train passages. Natural frequencies $f_{b1} = 8.1$ Hz and $f_{b3} = 9.5$ Hz are represented by horizontal solid and dashed lines, respectively. (b) Energy harvested and peak acceleration of the bridge response in $\mathcal{E}_1(7.8)$ and $\mathcal{E}_{0.5}(9.3)$ at measurement points $A14$ and $A23$.

passing in free vibration and d the load space. The dynamic response of the bridge at or near the resonant speed is mainly governed by the excited mode and at this the energy harvested is at a maximum [21]. The characteristic load space d is generally taken as the distance between bogies and can be found in [27].

The definition of the resonant speed can be expressed in terms of the bogie passing frequency V/d and its higher-order harmonics given by n. Thus, the bridge would exhibit a resonant behaviour when the bogie passing frequency, or its related higher-order harmonics, excites the natural frequencies. Fig. 15.(a) shows the bogie passing frequency and its related higher-order harmonics. The natural frequencies of the first and third modes are represented by horizontal lines to facilitate the interpretation of the results, and the load harmonics are represented by markers (diamond $n = 1$, circle $n = 2$, triangle $n = 3$, and square $n = 4$). Moreover, Fig. 15.(b) shows the peak value in the frequency content of the acceleration in the intervals $\mathcal{E}_1(7.8)$ and $\mathcal{E}_{0.5}(9.3)$ defined in Section 4.2 for each train passage (see Table 5). Also, the energy harvested is represented in this figure. High levels of vibration were observed for train passages with bogie passing frequency (or its related high-order harmonics) coinciding or close to the natural frequencies of the bridge. Overall the analysis showed the train passages excited the third mode shape more than the first one. The highest vibration levels occurred during passages #5, #7 and #18 when the related second harmonic of the load frequency was close to the third natural frequency of the bridge (circle markers matched the dashed line). These passages corresponded to the S102 configurations with speeds close to the resonant speed $V^r_{2,2} = 219.49$ km/h. Similarly, the train passages #6, #10 and #16 mainly excited the first mode shape and corresponded to the resonant speed $V^r_{1,2} = 184.49$ km/h for the S102 and S130 configurations (circle markers matched the solid line). Therefore, high levels of energy were obtained by harvesters tuned to f_{t1} and f_{t2} during these circulations.

In the following, the bridge response at point $A23$ and the output voltage generated by the harvester tuned to f_{t2} are analysed in detail for two train circulations. Fig. 16 shows the time history and frequency content of the bridge acceleration and output voltage induced by a Renfe S102-Duplex travelling at $V = 210.8$ km/h (passage #7). The second harmonic of the load was 8.91 Hz which is close to the tuning frequency $f_{t2} = 9.3$ Hz. The system response was then highly amplified, exhibiting a resonant behaviour as was observed in the voltage time history. The supplementary material in this article includes a recorded video of the harvester response during the train passage (`passage7.MOV`). The tip displacement is clearly observed. On the other hand, Fig. 17 shows that the response due to a Renfe S103 at $V = 116.0$ km/h (passage #9) was much lower than in the previous case. The train speed led to a low excitation frequency $V/d = 1.3$ Hz which is far from the natural frequencies of the bridge. The video recorded during the train passage shows low-amplitude tip displacement (see `passage9.MOV` video in the supplementary material). The energy harvested in passages #7 and #9 was 1.813 mJ and 0.066 mJ, respectively.

In addition, Figs. 16 and 17 also include a comparison of the output voltage estimated from the bridge acceleration and the experimental and analytical FRF's shown in Fig. 14. The time history shows higher amplification in the response estimated from the analytical FRF compared to those obtained from the experimental FRF, due to the slight differences in the damping ratio. The agreement of this estimation was acceptable close to the tuning frequency, although there were noticeable differences for higher frequencies as a result of the experimental estimation of the FRF. The energy harvested in passage #7 calculated from the analytical and experimental FRF's was 4.329 mJ and 2.586 mJ, respectively. Similarly, the energy harvested in passage #9 was 0.117 mJ and 0.089 mJ. Despite the inherent differences related to the experimental laboratory and in situ tests and the analytical model, the estimated results were acceptable for validating the proposed designs and the performance test in Section 4.3.

Next, the energy loss produced in systems tuned to the natural frequencies of the bridge is analysed using the analytical FRF's of the harvesters.

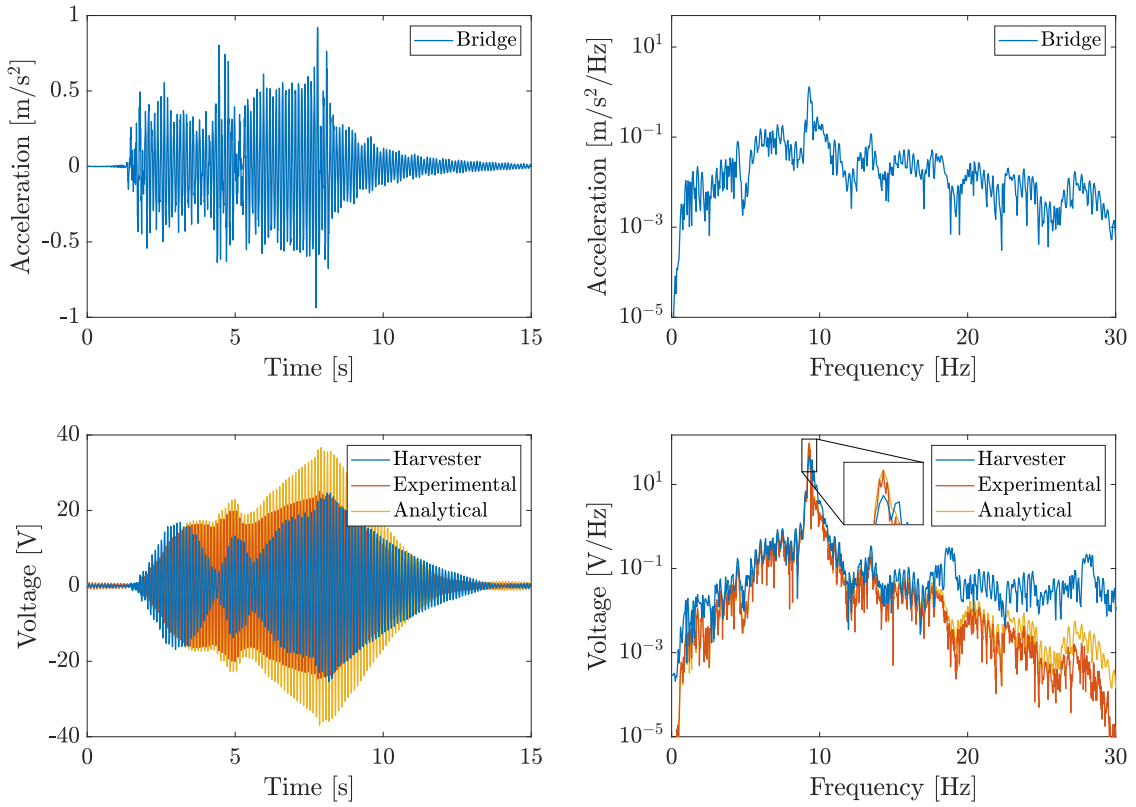

Fig. 16. Bridge acceleration and voltage at point $A23$ induced by Renfe S102-Duplex train circulating on track 3 at $V = 210.8$ km/h (passage #7). Estimated voltages from experimental and analytical FRF are also represented.

4.5. Energy loss due to tuning at natural frequencies

The energy loss due to detuning is assessed in this section comparing the performance of devices tuned at the optimal frequencies with the system tuned at the natural frequencies of the bridge. The harvested energy was estimated from the analytical FRF for voltage [25] and experimental acceleration on the bridge at the measurement points $A14$ and $A23$ (see Fig. 7).

Figs. 18 and 19 show the estimated time histories and frequency contents of the voltage produced by the harvesters tuned to the optimal frequencies $f_{t1} = 7.9$ Hz and $f_{t2} = 9.3$ Hz, and the corresponding to the devices tuned to the natural frequencies $f_{b1} = 8.1$ Hz and $f_{b3} = 9.5$ Hz, respectively. The train passages adequately excited the mode shapes to which the harvesters were tuned. In both cases, the voltage obtained from the harvesters tuned to the natural frequencies of the bridge was lower, with peak values 21.15 V/Hz for the tuning resonant frequency f_{b1} and 41.05 V/Hz for the optimal frequency f_{t1}, and 53.01 V/Hz and 112.36 V/Hz for f_{b3} and f_{t2}, respectively. The differences between the voltage levels were because the load frequency was closer to the optimal tuning frequencies.

The comparison for the 18 train passages showed the estimated energy harvested $\overline{E}_{t1} = 2.760$ mJ by the device tuned to f_{t1} was higher than the energy $\overline{E}_{b1} = 1.293$ mJ obtained from the harvester tuned to f_{b1}. Similarly, the results for the other device were $\overline{E}_{t2} = 12.369$ mJ and $\overline{E}_{b3} = 5.105$ mJ. The analysis of all train passages showed the systems tuned to the optimal tuning frequency and those tuned to the natural frequencies of the bridge produced similar energy levels when the mode shapes were not properly excited. These results highlight the influence of the tuning frequency on the harvested energy and validate the proposed procedure. Table 5 shows the energy harvested for all train passages. An overall analysis of the results showed the energy levels depend on the train passage, train configuration, and the travelling speed as was analysed in the previous section.

4.6. Discussion

The research presented in this article focuses on energy harvesting on high-speed train bridges, which are prone to high levels of transverse acceleration. A key issue in the proposed method is the number of train passages T_r used to estimate the optimal tuning frequency. A reliable estimate may require a sufficient sample size to adequately represent the operating conditions of a railway line. High-speed lines operate under very stable conditions of speed and train type [27,47]. Therefore, the measurement time window for estimating the tuning frequency could be considerably shorter than on conventional or freight lines where the variability of operating conditions is greater.

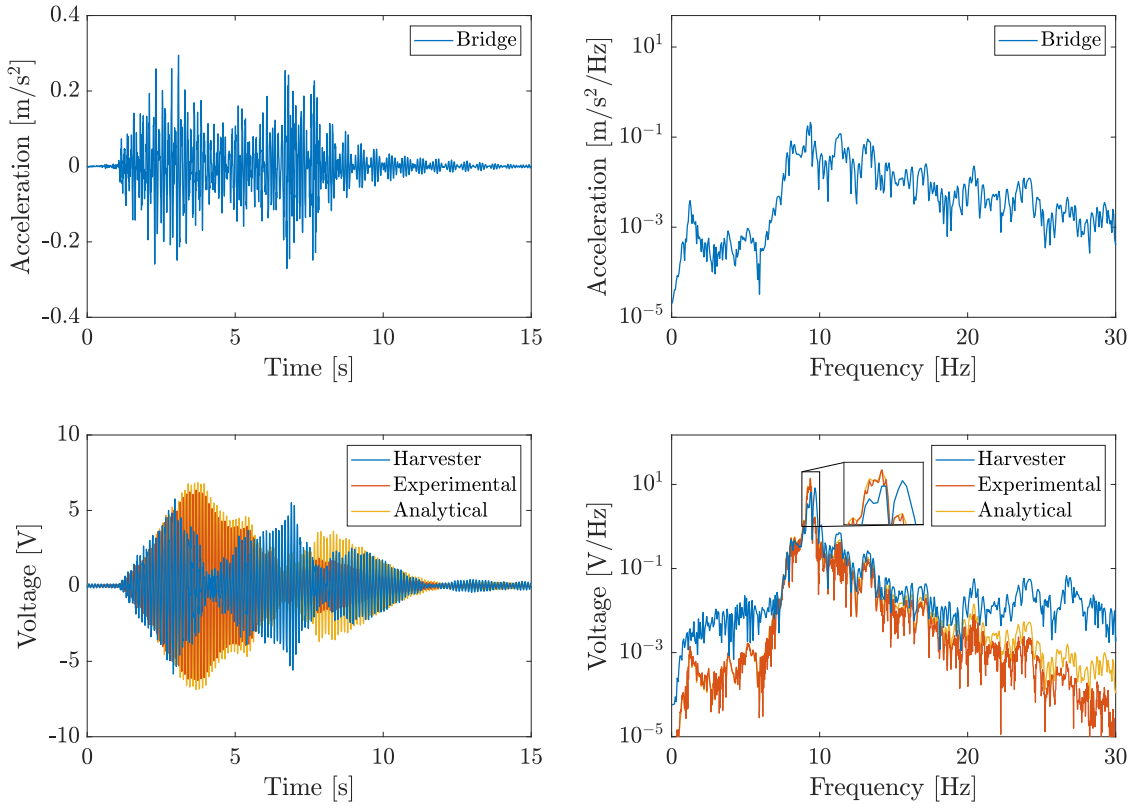

Fig. 17. Bridge acceleration and voltage at point $A23$ induced by Renfe S103 train circulating on track 2 at $V = 116.0$ km/h (passage #9). Estimated voltages from experimental and analytical FRF are also represented.

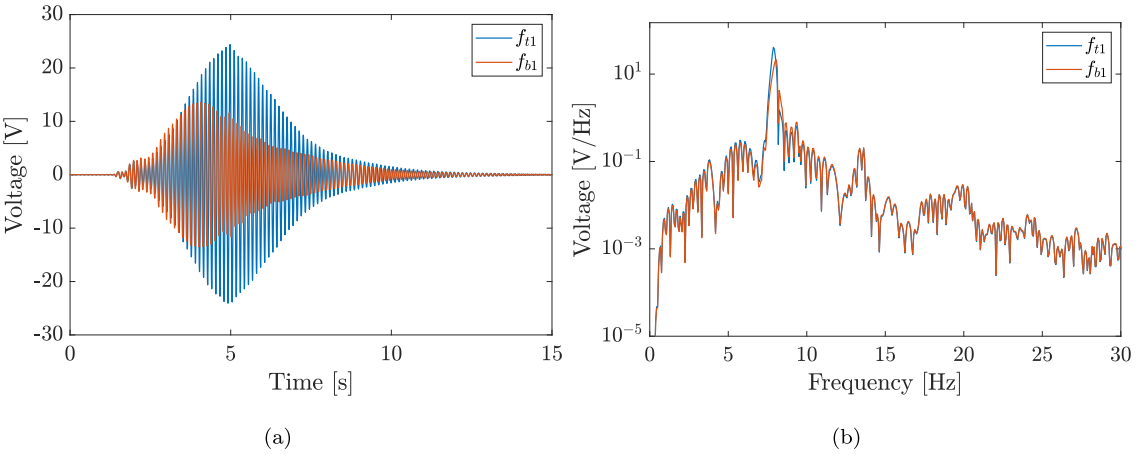

Fig. 18. (a) Time history and (b) frequency content of the voltage generated by a harvester located at point $A14$ induced by a Renfe S102 train circulating on track 2 at $V = 177.8$ km/h (passage #6).

Following, the results of a convergence analysis in the estimation of optimal tuning frequencies are presented. Fig. 20 shows the convergence of the tuning frequency. The train passages of both stages were analysed together to increase the sample size. The tuning frequency was subsequently estimated at each train passage, increasing the sample size with the previous one. Fig. 20.(a) shows the relative error in the estimation of the tuning frequency compared to the optimal values $f_{t1} = 7.9$ Hz and $f_{t2} = 9.3$ Hz. The maximum error is below 5% and is almost constant around 2% after passage #15. The shaded area corresponds to the passages measured in the first stage, while the unshaded area corresponds to those recorded in the second stage. Furthermore, the coefficient R^2 was analysed to evaluate the fitness of the peak energy frequencies to the normal distribution $N(\hat{\mu}, \hat{\sigma})$ defined in Section 2.1.

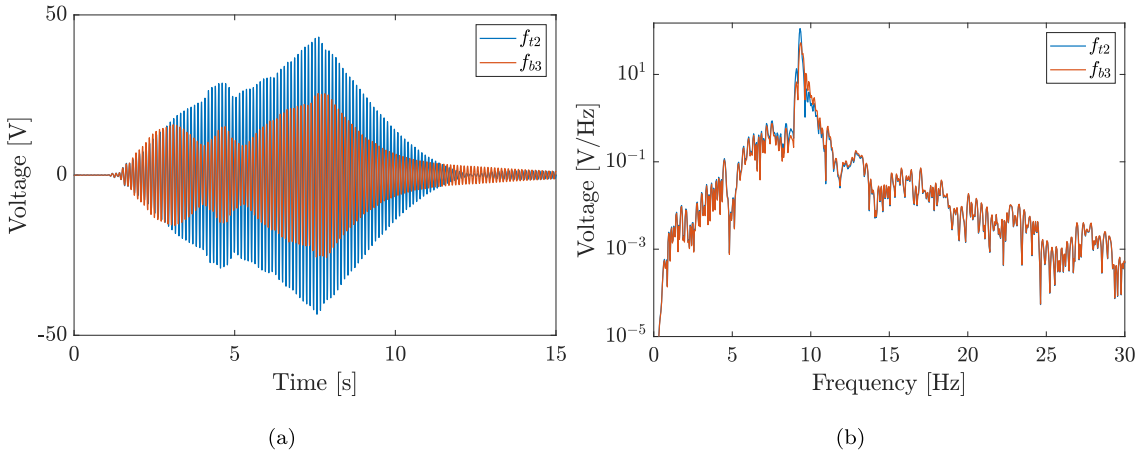

Fig. 19. (a) Time history and (b) frequency content of the voltage generated by a harvester located at point $A23$ induced by a Renfe S102 train in duplex configuration circulating on track 3 at $V = 211.4$ km/h (passage #18).

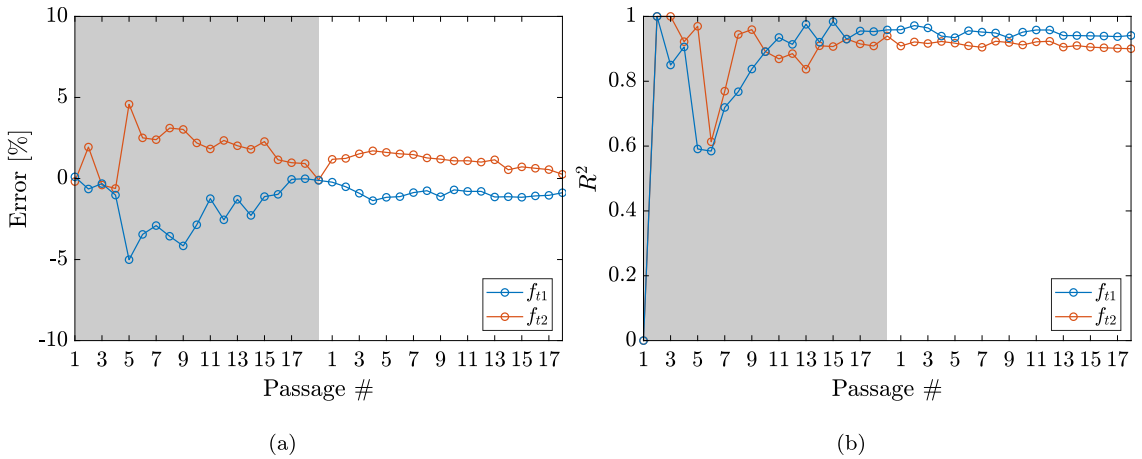

Fig. 20. (a) Relative error in tuning frequency estimation and (b) determination coefficient R^2 for different train passages measured in first stage (shaded area) and second stage (unshaded area).

The results of this analysis concluded that the number of train passages during the first stage was sufficient to provide a reliable estimate of the tuning frequency.

5. Conclusions

This research proposed and validated a new tuning strategy for energy harvesters on railway bridges. The procedure is based on the statistical distribution of the mechanical energy generated by a lumped-mass model subjected to bridge vibrations under operating conditions. It was found the mechanical energy produced by a harvester tuned over a frequency range presented peak values close to the natural frequencies of the bridge that depend on the train configuration and speed. The energy levels followed a Gamma distribution and the peak energy frequencies a Gaussian distribution. The mean value of the peak energy frequencies corresponded to the tuning frequency that maximised the harvester performance. The estimated tuning frequencies were slightly lower than the natural frequency of the bridge in all cases studied.

The proposed procedure has been experimentally validated on a railway bridge on a high-speed line in service. The experimental tests consisted, in the first stage, of the measurement of vibrations produced by railway traffic to identify the tuning frequency, the manufacturing, and the laboratory test of energy harvesters. Later, the performance of the devices were evaluated under real operating conditions. The tuning frequencies were approximately 4–7% lower than the natural frequencies of the bridge to which the devices were tuned, and the energy harvested increased up to 300% using the proposed method. Furthermore, the energy level depended on the train configuration and speed. The maximum energy occurred when the train speed was close to a resonant speed. The total energy harvested in a time window of three hours (18 train passages) was 7.65 mJ.

The proposed approach is well suited to high-speed lines because the railway traffic is more homogeneous in terms of train types and travelling speed. The identification of tuning frequencies in bridges of conventional lines could be more uncertain due to the wide range of trains (e.g. freight) and operational conditions.

CRediT authorship contribution statement

J.C. Cámara-Molina: Conceptualization, Methodology, Software, Investigation, Validation, Writing – original draft, Writing – review & editing. **A. Romero:** Conceptualization, Methodology, Software, Investigation, Validation, Funding acquisition, Supervision, Writing – original draft, Writing – review & editing. **E. Moliner:** Investigation, Validation, Writing – original draft, Writing – review & editing. **D.P. Connolly:** Supervision, Writing – original draft, Writing – review & editing. **M.D. Martínez-Rodrigo:** Conceptualization, Investigation, Validation, Funding acquisition, Writing – original draft, Writing – review & editing. **D. Yurchenko:** Supervision, Writing – original draft, Writing – review & editing. **P. Galvín:** Conceptualization, Methodology, Software, Investigation, Validation, Funding acquisition, Writing – original draft, Writing – review & editing.

Declaration of competing interest

The authors declare that they have no known competing financial interests or personal relationships that could have appeared to influence the work reported in this paper.

Data availability

Data will be made available on request.

Acknowledgements

The authors would like to acknowledge the financial support provided by the Spanish Ministry of Science, Innovation and Universities under the research project PID2019-109622RB; Spanish Ministry of Science and Innovation under the research project PID2022-138674OB; PROYEXCEL_00659 funded by Regional Ministry of Economic Transformation, Industry, Knowledge and Universities of Andalusia; Generalitat Valenciana, Spain under the research project AICO/2021/200, and the Andalusian Scientific Computing Centre (CICA).

Appendix A. Supplementary data

Supplementary material related to this article can be found online at https://doi.org/10.1016/j.ymssp.2023.111012.

References

[1] L. Atzori, A. Iera, G. Morabito, The internet of things: A survey, Comput. Netw. 54 (2010) 2787–2805.
[2] S. Li, L.D. Xu, S. Zhao, The internet of things: a survey, Inf. Syst. Front. 17 (2015) 243–259.
[3] D. Abruzzese, A. Micheletti, A. Tiero, M. Cosentino, D. Forconi, G. Grizzi, G. Scarano, S. Vuth, P. Abiuso, IoT sensors for modern structural health monitoring. A new frontier, Procedia Struct. Integr. 25 (2020) 378–385.
[4] F. Lamonaca, P.F. Sciammarella, C. Scuro, D.L. Carni, R.S. Olivito, Internet of things for structural health monitoring, in: 2018 Workshop on Metrology for Industry 4.0 and IoT, MetroInd 4.0 and IoT 2018 - Proceedings, 2018, pp. 95–100.
[5] A. Abdelgawad, K. Yelamarthi, Internet of things (IoT) platform for structure health monitoring, Wirel. Commun. Mob. Comput. 2017 (2017).
[6] D. Barke, K.W. Chiu, Structural health monitoring in the railway industry: A review, Struct. Health Monit. 4 (1) (2005) 81–94.
[7] M. Vagnoli, R. Remenyte-Prescott, J. Andrews, Railway bridge structural health monitoring and fault detection: State-of-the-art methods and future challenges, Struct. Health Monit. 17 (4) (2018) 971–1007.
[8] G. Jing, M. Siahkouhi, J.R. Edwards, M.S. Dersch, N.A. Hoult, Smart railway sleepers - A review of recent developments, challenges, and future prospects, Constr. Build. Mater. 271 (2021) 121533.
[9] T. Yildirim, M.H. Ghayesh, W. Li, G. Alici, A review on performance enhancement techniques for ambient vibration energy harvesters, Renew. Sustain. Energy Rev. 71 (2017) 435–449.
[10] C. Wei, X. Jing, A comprehensive review on vibration energy harvesting: Modelling and realization, Renew. Sustain. Energy Rev. 74 (2017) 1–18.
[11] Y. Li, K. Tao, B. George, Z. Tan, Harvesting vibration energy: Technologies and challenges, IEEE Ind. Electron. Mag. 15 (2021) 30–39.
[12] J.C. Rodriguez, V. Nico, J. Punch, A vibration energy harvester and power management solution for battery-free operation of wireless sensor nodes, Sensors 19 (17) (2019) 3776.
[13] A. Erturk, D.J. Inman, Broadband piezoelectric power generation on high-energy orbits of the bistable Duffing oscillator with electromechanical coupling, J. Sound Vib. 330 (10) (2011) 2339–2353.
[14] S.W. Ibrahim, W.G. Ali, A review on frequency tuning methods for piezoelectric energy harvesting systems, J. Renew. Sustain. Energy 4 (2012) 062703.
[15] L. Tang, Y. Yang, C.K. Soh, Toward broadband vibration-based energy harvesting, J. Intell. Mater. Syst. Struct. 21 (18) (2010) 1867–1897.
[16] C. Eichhorn, F. Goldschmidtboeing, P. Woias, Bidirectional frequency tuning of a piezoelectric energy converter based on a cantilever beam, J. Micromech. Microeng. 19 (2009).
[17] Y. Cheng, N. Wu, Q. Wang, An efficient piezoelectric energy harvester with frequency self-tuning, J. Sound Vib. 396 (2017) 69–82.
[18] W. Al-Ashtari, M. Hunstig, T. Hemsel, W. Sextro, Increasing the power of piezoelectric energy harvesters by magnetic stiffening, J. Intell. Mater. Syst. Struct. 24 (11) (2013) 1332–1342.
[19] C.V. Karadag, N. Topaloglu, Aself-sufficient and frequency tunable piezoelectric vibration energy harvester, J. Vib. Acoust. Trans. ASME 139 (1) (2017).
[20] S.A. Kouritem, M.A. Bani-Hani, M. Beshir, M.M. Elshabasy, W.A. Altabey, Automatic resonance tuning technique for an ultra-broadband piezoelectric energy harvester, Energies 15 (2022) 7271.

[21] A. Romero, J.C. Cámara-Molina, E. Moliner, P. Galvín, M.D. Martínez-Rodrigo, Energy harvesting analysis in railway bridges: An approach based on modal decomposition, Mech. Syst. Signal Process. 160 (2021).
[22] P. Cahill, N.A.N. Nuallain, N. Jackson, A. Mathewson, R. Karoumi, V. Pakrashi, Energy harvesting from train-induced response in bridges, J. Bridge Eng. 19 (9) (2014).
[23] F.U. Khan, I. Ahmad, Review of energy harvesters utilizing bridge vibrations, Shock Vib. 2016 (2016).
[24] Y. Song, Finite-element implementation of piezoelectric energy harvesting system from vibrations of railway bridge, J. Energy Eng. 145 (2) (2019).
[25] J.C. Cámara-Molina, E. Moliner, M. Martínez-Rodrigo, D. Connolly, D. Yurchenko, P. Galvín, A. Romero, 3D printed energy harvesters for railway bridges-design optimisation, Mech. Syst. Signal Process. 190 (2023) 110133.
[26] A. Zangeneh, C. Svedholm, A. Andersson, C. Pacoste, R. Karoumi, Identification of soil–structure interaction effect in a portal frame railway bridge through full-scale dynamic testing, Eng. Struct. 159 (2018) 299–309.
[27] P. Galvín, A. Romero, E. Moliner, G. De Roeck, M.D. Martínez-Rodrigo, On the dynamic characterisation of railway bridges through experimental testing, Eng. Struct. 226 (2020).
[28] N. Stephen, On energy harvesting from ambient vibration, J. Sound Vib. 293 (1) (2006) 409–425.
[29] J.M. Rocha, A.A. Henriques, R. Calçada, Safety assessment of a short span railway bridge for high-speed traffic using simulation techniques, Eng. Struct. 40 (2012) 141–154.
[30] F. Zakęś, P. Śniady, Vibrations of a multi-span beam subjected to a moving stochastic load, in: Springer Proceedings in Mathematics and Statistics, Vol. 248, 2018, pp. 403–413.
[31] G. Lombaert, P. Galvín, S. François, G. Degrande, Quantification of uncertainty in the prediction of railway induced ground vibration due to the use of statistical track unevenness data, J. Sound Vib. 333 (18) (2014) 4232–4253.
[32] M.F. Daqaq, Characterizing the response of galloping energy harvesters using actual wind statistics, J. Sound Vib. 357 (2015) 365–376.
[33] O. Gaidai, Y. Cao, Y. Xing, J. Wang, Piezoelectric energy harvester response statistics, Micromachines 14 (2023) 271.
[34] C. Lee, F. Famoye, A.Y. Alzaatreh, Methods for generating families of univariate continuous distributions in the recent decades, WIREs Comput. Stat. 5 (2013) 219–238.
[35] Z.-S. Ye, N. Chen, Closed-form estimators for the Gamma distribution derived from likelihood equations, Amer. Statist. 71 (2017) 177–181.
[36] H.S. Klakattawi, The Weibull-Gamma distribution: Properties and applications, Entropy 21 (2019) 438.
[37] G. Marsaglia, W. Tsang, J. Wang, Evaluating Kolmogorov's distribution, J. Stat. Softw. 8 (18) (2003).
[38] J. Chordà-Monsonís, A. Romero, E. Moliner, P. Galvín, M.D. Martínez-Rodrigo, Ballast shear effects on the dynamic response of railway bridges, Eng. Struct. 272 (2022) 114957.
[39] M.D. Martínez-Rodrigo, E. Moliner, A. Romero, G. De Roeck, P. Galvín, Maximum resonance and cancellation phenomena in orthotropic plates traversed by moving loads: Application to railway bridges, Int. J. Mech. Sci. 169 (2020) 105316.
[40] E. Moliner, M.D. Martínez-Rodrigo, P. Galvín, J. Chordà-Monsonís, A. Romero, On the vertical coupling effect of ballasted tracks in multi-span simply-supported railway bridges under operating conditions, Struct. Infrastruct. Eng. (2022).
[41] R. Brincker, L. Zhang, P. Andersen, Modal identification of output-only systems using frequency domain decomposition, Smart Mater. Struct. 10 (3) (2001) 441–445.
[42] R. Brincker, C.E. Ventura, Introduction To Operational Modal Analysis, John Wiley & Sons Ltd, 2015.
[43] P-876 DuraAct patch transducer information, https://www.piceramic.com/en/products/piezoceramic-actuators/patch-transducers/p-876-duraact-patch-transducer-101790/.
[44] Ultrafuse filamnets, https://www.ultrafusefff.com.
[45] ASTM designation: D638—14 standard test method for tensile properties of plastics, 2014.
[46] G.A.F. Seber, C.J. Wild, Nonlinear Regression, Wiley-Interscience, Hoboken, NJ, 2003.
[47] P. Galvín, A. Romero, E. Moliner, M.D. Martínez-Rodrigo, Two FE models to analyse the dynamic response of short span simply-supported oblique high-speed railway bridges: Comparison and experimental validation, Eng. Struct. 167 (2018) 48–64.